An observationally based constraint on the water-vapor feedback

N. D. Gordon,[1] A. K. Jonko,[2] P. M. Forster,[3] and K. M. Shell[4]

Received 13 May 2013; revised 13 September 2013; accepted 21 October 2013; published 22 November 2013.

[1] The increase in atmospheric concentrations of water vapor with global warming is a large positive feedback in the climate system. Thus, even relatively small errors in its magnitude can lead to large uncertainties in predicting climate response to anthropogenic forcing. This study incorporates observed variability of water vapor over 2002–2009 from the Atmospheric Infrared Sounder instrument into a radiative transfer scheme to provide constraints on this feedback. We derive a short-term water vapor feedback of 2.2 ± 0.4 $Wm^{-2}K^{-1}$. Based on the relationship between feedback derived over short and long timescales in twentieth century simulations of 14 climate models, we estimate a range of likely values for the long-term twentieth century water vapor feedback of 1.9 to 2.8 $Wm^{-2}K^{-1}$. We use the twentieth century simulations to determine the record length necessary for the short-term feedback to approach the long-term value. In most of the climate models we analyze, the short-term feedback converges to within 15% of its long-term value after 25 years, implying that a longer observational record is necessary to accurately estimate the water vapor feedback.

Citation: Gordon, N. D., A. K. Jonko, P. M. Forster, and K. M. Shell (2013), An observationally based constraint on the water-vapor feedback, *J. Geophys. Res. Atmos.*, *118*, 12,435–12,443, doi:10.1002/2013JD020184.

1. Introduction

[2] In a warming climate, the amount of water vapor in the atmosphere is expected to increase, amplifying the greenhouse effect. This water vapor feedback is consistently found to be the largest positive feedback in global climate models [e.g., *Colman*, 2003; *Soden and Held*, 2006, hereafter SH06], with the potential to double any warming produced by an external forcing. However, model intercomparison studies produce a range in feedback values, and uncertainty about the exact magnitude of this feedback persists. Thus, an effort has been underway to constrain this, as well as other feedbacks, using observations. However, the relatively short satellite data record of global, vertically resolved water vapor has made observational studies prone to large uncertainties and raises questions about the relationship between feedbacks resulting from transient warming and short-term variability.

[3] *Hall and Manabe* [1999] diagnose an interannual water vapor feedback in the Geophysical Fluid Dynamics Laboratory (GFDL) climate model, and *Colman and Power* [2009] use the Bureau of Meteorology Research Centre coupled model version 2.2 to compare the water vapor feedback generated by interannual variability to a transient warming feedback. Both find the short-term water vapor feedback to be positive, but it appears to be smaller in magnitude and noisier than the transient warming feedback [*Colman and Power*, 2009]. An increasing number of studies have derived the water vapor feedback due to different types of forcing directly from observations. *Soden et al.* [2002] and *Forster and Collins* [2004] use the climate response to the eruption of Mount Pinatubo in 1991 to diagnose a positive water vapor feedback in response to an external perturbation, while *Soden* [1997] and *Dessler et al.* [2008, hereafter D08] calculate a feedback using internal variability due to El Niño-Southern Oscillation (ENSO) as the forcing. While earlier studies were limited to observations of top-of-atmosphere radiative fluxes to examine changes in greenhouse trapping, the availability of atmospheric profiles of water vapor and temperature from the Atmospheric Infrared Sounder (AIRS) has made direct estimates of the water vapor feedback possible [D08; *Gettelman and Fu*, 2008].

[4] The present study advances D08, by including (a) an alternative feedback analysis technique, (b) additional satellite data, and (c) a comparison with climate models to help place constraints on long-term feedback. In addition, we use long-term climate model simulations to determine the record length necessary for a short-term feedback estimate to approach the long-term feedback value.

2. Methods

[5] As the Earth surface warms in response to an external forcing, several feedback mechanisms act to increase

[1]Lawrence Livermore National Laboratory, Livermore, California, USA.
[2]National Center for Atmospheric Research, Boulder, Colorado, USA.
[3]School of Earth and Environment, University of Leeds, Leeds, UK.
[4]College of Earth, Ocean and Atmospheric Sciences, Oregon State University, Corvallis, Oregon, USA.

Corresponding author: N. D. Gordon, Lawrence Livermore National Laboratory, 7000 East Ave., Livermore, CA 94550, USA. (gordon40@llnl.gov)

2169-897X/13/10.1002/2013JD020184

or dampen the initial surface warming. As in *Forster and Taylor* [2006], we define a globally averaged feedback parameter (Y)

$$Y = \frac{dN}{dT_s} \tag{1}$$

In this equation, dT_s is the global mean above-surface temperature perturbation and dN is the globally averaged net (longwave plus shortwave) top-of-atmosphere (TOA) irradiance change due to the climate change resulting from a temperature perturbation dT_s. *Forster and Taylor* [2006] have shown that linear feedback analysis is an effective tool for estimating climate sensitivity in long runs of global climate models, although multiple uncertainties exist when such an approach is applied to short-term observations, as in *Forster and Gregory* [2006] [e.g., *Spencer and Braswell*, 2008; *Murphy and Forster*, 2010].

[6] The feedback parameter, Y, can be broken down into several components, each representing a different process in the climate system, including changes in surface albedo, lapse rate, water vapor, and clouds. In this formalism, the water vapor feedback is represented by

$$Y_q = \frac{dN_q}{dT_s} = \frac{\partial N_q}{\partial q}\frac{dq}{dT_s} \tag{2}$$

Here, dq/dT_s represents the water vapor response to the temperature perturbation, while $\partial N_q/\partial q$ is the net global mean TOA irradiance change caused by the associated change in water vapor content.

[7] Several different methods to estimate water vapor feedback based on equation (2) have been developed to date.

[8] 1. The Partial Radiative Perturbation method (PRP) [*Wetherald and Manabe*, 1988; *Colman*, 2003] uses an offline radiative transfer model to calculate dN_q/dT_s by swapping the three-dimensional water vapor fields between two climate states, while all other climate variables are held constant. The radiation code computes TOA radiative fluxes for a control climate and again for the same control climate with the water vapor field substituted from a perturbed climate state. The difference between the two calculations, dN_q, is divided by the globally averaged surface temperature change.

[9] 2. The radiative kernel technique [SH06; D08; *Soden et al.*, 2008; *Shell et al.*, 2008] separately calculates the two derivatives in equation (2), using the natural logarithm of specific humidity as the climate variable. The method uses an offline radiation code to calculate the radiative impact of a unit change in water vapor at each latitude, longitude, and vertical level for each month. The feedback term is then estimated by multiplying this "kernel" at each point by the actual water vapor change between two climate states at that latitude, longitude, vertical level, and month and dividing by the global mean above-surface temperature change.

[10] 3. *Forster and Gregory* [2006] use linear regression of globally averaged clear-sky longwave TOA flux against global mean temperature to diagnose feedback from short-term interannual variability. They assume that the clear-sky longwave regression slope combines a known Planck response with a water vapor and lapse rate feedback term.

[11] In this paper, we estimate the water vapor feedback from temperature changes associated with interannual variability using a combination of PRP and regression analysis. In the PRP-type approach, we calculate a time series of the global integral of

$$dN_q = \frac{\partial N}{\partial q}dq \tag{3}$$

by varying monthly, three-dimensional water vapor fields in an offline radiative transfer code, whilst keeping the rest of the radiation code inputs at their climatological values. This uses a single PRP calculation, rather than a pair of calculations as sometimes used when analyzing feedback in 2×CO2 studies [e.g., *Colman and McAvaney*, 2009], as we perform calculations about a monthly base state and an anomaly field. The time series of globally averaged TOA flux anomaly is regressed against global mean above-surface temperature to determine the water vapor feedback. For comparison, we also use the radiative kernel approach to calculate a time series of dN_q in equation (3) (referred to as dN_{kq}) and calculate the corresponding feedback.

[12] All PRP calculations are performed with the Edwards-Slingo (ES) radiation code [*Edwards and Slingo*, 1996], as used in the UK Met Office weather and climate models. It is a two-stream radiation code that, given the distribution of surface albedo and radiatively important constituents of the atmosphere, calculates the transfer of solar and terrestrial radiation through the atmosphere. For each month for which satellite observations of water vapor are available, we run the radiation code, fixing all nonwater vapor variables at a monthly averaged climatology. We obtain the monthly climatology from the European Centre for Medium-Range Weather Forecasts' ERA-40 reanalysis data [*Uppala et al.*, 2005], with the exception of cloud fields, which are derived from 21 years of data from the International Satellite Cloud Climatology Project [*Rossow and Schiffer*, 1999]. This setup follows that of *Rap et al.* [2010].

3. Data

[13] *Water Vapor.* Water vapor profiles are derived from the Atmospheric Infrared Sounder (AIRS) instrument aboard the Aqua satellite in a near-polar orbit. This vertically resolved water vapor product has an accuracy for the total column of 10% over ocean and 30% over land, when compared to sondes and Advanced Microwave Scanning Radiometer-EOS [*Fetzer et al.*, 2005]. The root-mean-square error (RMSE) between sondes and AIRS is 12% in the free troposphere, and near 30% for surface values [*Fetzer et al.*, 2005]. While errors can be large for absolute measurements, we consider anomalies of water vapor, for which errors should be smaller. Further, errors are largest near the surface and over land. However, changes relevant to water vapor feedback occur in the upper troposphere, and only 30% of the Earth's surface is covered by land, which further reduces the error relevant to our analysis. Another caveat to our calculations is that AIRS does not retrieve water vapor in overcast situations. Retrievals can only be made in situations with up to 80% cloud cover [*Susskind et al.*, 2003]. The result is a dry bias, since no data is obtained for situations that have the highest water vapor content. This means that our calculations potentially underestimate the true water vapor feedback.

[14] We utilize the level-3 AIRS product, which collects the observations into monthly means from September 2002

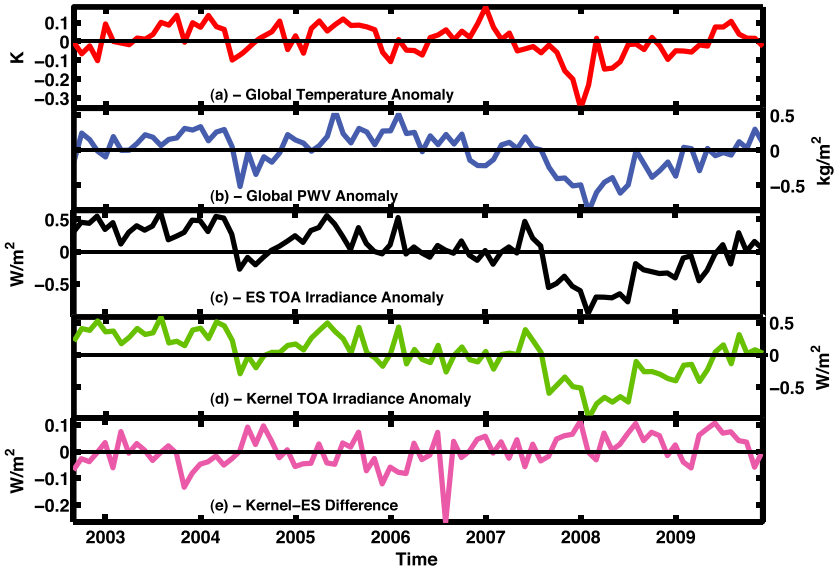

Figure 1. Time series for the AIRS observational period (September 2002–December 2009) of (a) global mean surface temperature anomaly (with respect to mean of time period) from HadCRUT3 data set, (b) AIRS-derived global mean precipitable water vapor anomaly, and global mean TOA net irradiance anomaly derived from (c) full integration of the radiation code, (d) kernel calculation, and (e) difference (kernel-ES).

to December 2009 for each 1 × 1° grid box over the globe, and we use both the ascending and descending nodes. The AIRS instrument provides water vapor at six vertical layers in the atmosphere (1000, 850, 700, 500, 300, and 100 hPa). Figure 1b shows the global mean column-integrated precipitable water vapor (PWV) anomaly as observed by the AIRS instrument for the time period of available data. All time series are the monthly anomalies relative to the climatology over our time period of observation.

[15] *Surface Temperature.* We employ Version 3 of the UK Met Office Hadley Centre-Climate Research Unit (University of East Anglia) variance-adjusted surface temperature data set [*Brohan et al.*, 2005; HadCRUT3]. Our analysis technique is similar to the method of D08, who calculate the feedback parameter using the change in global mean water vapor from five Januarys relative to January 2008, which was subject to relatively cool and dry La Niña conditions. Our analysis builds on these results but uses the entire available AIRS data set and all months, and we use global, as opposed to tropical, mean surface temperature as the regressor, as this is more consistent with traditional definitions of global feedback. We have repeated the analysis using tropical averages of surface temperature as well as different surface temperature data sets and found similar results (not shown). The time series of the global mean temperature anomalies with respect to the AIRS time period is shown in Figure 1a.

4. Short-Term Feedback Analysis

[16] For illustrative purposes, Figure 2a shows a scatterplot of global mean TOA flux anomaly (dN_q) and global mean precipitable water vapor anomaly (dq), and Figure 2b is a scatterplot of anomalous precipitable water vapor and global mean temperature from HadCRUT3. The regression lines represent ordinary least squares (OLS) fit to the data, giving rough global approximations to the $\partial N/\partial q$ (with slope 1.1 Wm^{-2} per kg m^{-2}) and dq/dT_s (with slope 1.5 kg m^{-2} per K) terms in equation (2). The relationship in Figure 2a appears more linear than that in Figure 2b. Note that these regressions merely suggest applicability of linear feedback analysis. Simply multiplying these two area-averaged slopes together would give an incorrect value for water vapor feedback, because the two terms ($\partial N/\partial q$ and dq) are spatially correlated. Here we do not use these slopes to estimate dN_q/dT_s. Rather, we obtain estimates of $dN_q = \partial N_q/\partial q\, dq$ in two ways and then regress against dT_s. To obtain the PRP estimate, we run the ES radiation code twice—first with climatological monthly mean water vapor content, and then with monthly varying water vapor from January 2002 to December 2009—and take the difference in TOA irradiance, dN_q (Figure 1c). The net TOA flux anomaly here is dominated by variability in longwave fluxes. The shortwave flux variability is well correlated to the longwave and an order of magnitude smaller (not shown).

[17] Next, an equivalent time series of dN_{kq} is calculated using the kernel technique as described in *Soden et al.* [2008] (Figure 1d). In order to make the kernel results directly comparable to our full radiative transfer calculations, we derive a kernel using satellite observations, rather than climate model data, as the base state. We utilize the climatological monthly AIRS water vapor and atmospheric temperature as input for the ES radiation code, perturbing the water vapor at each location and atmospheric level to calculate the effect of water vapor on TOA radiation, creating a "data kernel" (Figure 3). As with previous derivations of radiative kernels, the unit perturbation in water vapor is that which would maintain constant relative humidity for a 1 K temperature increase, hereafter referred to as q_{1K}. To mirror the technique of *Soden et al.* [2008] and *Shell et al.* [2008], the relationship between water vapor and radiation is computed for ln(q), since absorption of radiation by water vapor

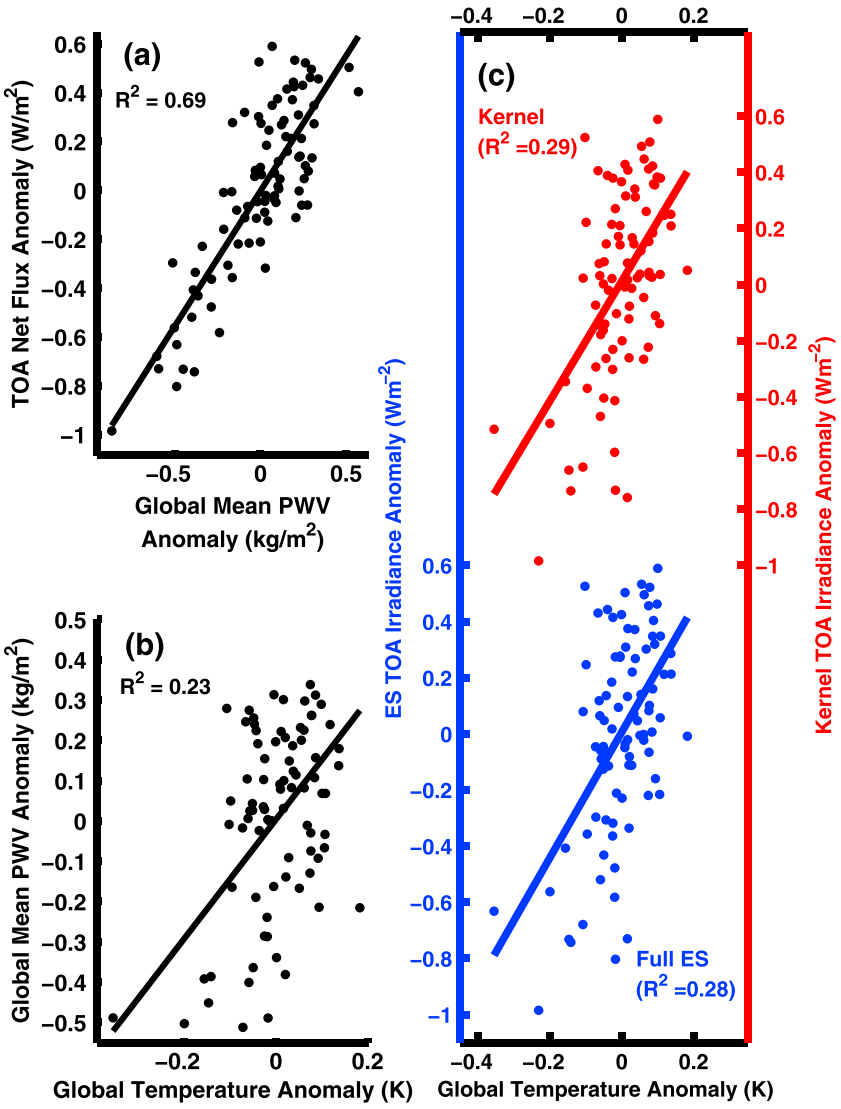

Figure 2. Regressions of (a) satellite-derived global mean precipitable water vapor anomaly and simulated TOA net irradiance anomaly from the radiation code, (b) global mean surface temperature and global mean precipitable water vapor, and (c) global mean surface temperature from HadCRUT3 and TOA net irradiance anomaly for the full radiation code (blue) and for the kernel technique (red).

scales with ln(q) [e.g., *Held and Soden*, 2000]. Equation (3) becomes $dN_q = \frac{\partial N}{\partial ln(q)} d(ln(q))$, and we divide ∂N from the data kernel calculation by $ln(q_{base} + q_{1K}) - ln(q_{base})$ to obtain the first term.

[18] The water vapor kernel derived from AIRS observations is similar to those derived from model fields in previous research [SH06, *Soden et al.*, 2008]. For comparison, we have also calculated a time series using the same kernel as in *Shell et al.* [2008]. The two kernels give similar globally averaged TOA flux anomalies (not shown). The advantage of the kernel technique is that, once the radiation code has been run for a unit perturbation, one can then calculate the change in TOA radiation that results from all months of observed perturbation in water vapor simply by multiplying them by the kernel. However, the kernel technique does treat each layer independently when calculating the effect that a given perturbation has on TOA flux, and we observe that perturbations in water vapor are vertically coherent in both interannual and climate change scenarios (Figure 4). Figure 1e shows the time series of the difference between the data kernel and full radiation code. Because the irradiance anomalies fluctuate around 0, there are individual months for which the difference between the two methods is large. However, if we consider those months that have an irradiance anomaly larger than one standard deviation from the mean, this difference amounts to < 10% of the anomaly itself.

[19] Our global feedback estimates are shown in Figure 2c for the full radiation scheme (blue dots) and kernel method (red dots). The skill values of the regressions are $R^2 = 0.29$ for the kernel technique and $R^2 = 0.28$ for the full ES. With a sample size of 88, both are statistically significant at $\alpha = 0.01$ or 99% significance level. We thus consider the linear feedback model to be a reasonable assumption, although there is some evidence in Figure 2c for a stronger response at higher surface temperatures, i.e., more data points lie

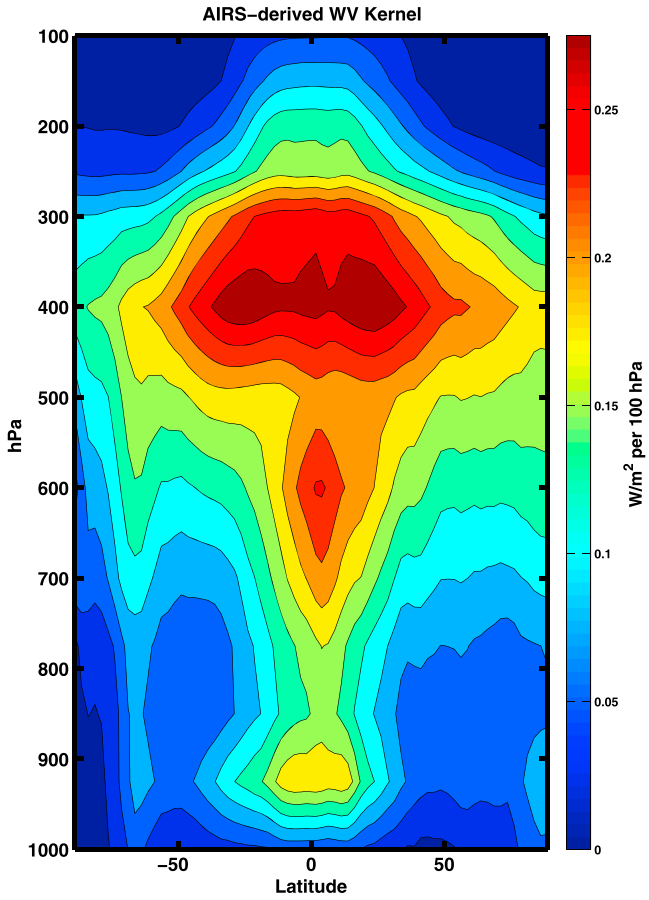

Figure 3. Zonal average of change in net TOA irradiance for a unit perturbation in water vapor that corresponds to a 1 K temperature change with fixed relative humidity (Wm^{-2} per 100 mb).

above the regression line. This is consistent with *Colman and McAvaney* [2009] and *Jonko et al.* [2013] who find an increase of water vapor feedback strength in warmer climates. However, we do not have enough independent points to constrain higher order moments. So, for simplicity, we adopt a linear feedback analysis, where slopes of the OLS regression lines in Figure 2c represent Y_q in equation (2). We employ a bootstrapping method to calculate the regression coefficients and their errors, whereby we sample n_{eff} months with replacement, where n_{eff} is our effective number of monthly integrations, accounting for auto correlation in the data. The autocorrelation of the monthly temperature anomaly falls below a value of 0.5 after a 2 month lag; and to account for this, we assume that data points are only independent after 4 months, reducing the effective number of points to 22. We then carry out ordinary least squares calculations [*Feigelson and Babu*, 1992]. We repeat this process 10,000 times and calculate the mean and 95% confidence interval of the regression coefficient from this distribution. Applying this technique to the AIRS observations gives a water-vapor feedback estimate of 2.19 ± 0.38 $Wm^{-2}K^{-1}$ when using the full ES radiative calculations. Using the kernel technique, we calculate a very similar feedback of 2.14 ± 0.37 $Wm^{-2}K^{-1}$. D08, using January AIRS data and the kernel method, estimate a water vapor feedback factor of 2.04 $Wm^{-2}K^{-1}$. *Forster and Gregory* [2006] use the cooling associated with the eruption of Mt. Pinatubo to estimate a feedback between 0.9 and 2.5 $Wm^{-2}K^{-1}$. Our calculation of this feedback using partial radiative perturbations is similar to, but at the high end of, the longer-term water vapor feedback calculated from climate model simulations of the 21st century using the kernel technique (1.5–2.1 $Wm^{-2}K^{-1}$) [SH06].

[20] A major source of uncertainty arises from the fact that our data record is relatively short. *Colman and Power* [2009] calculate the water vapor feedback using the PRP method for both natural variability and transient climate change. They find that the feedback derived from natural variability is about two thirds of that in response to transient greenhouse gas forcing. While our record includes the response of the climate to increasing greenhouse gases, interannual variability, namely the relatively cold La Niña of 2008, has a major influence on our results. The variability in water vapor distribution due to interannual fluctuations is different than that resulting from long-term weakly forced (transient) changes [*Colman and Hanson*, 2013; *Dalton and Shell*, 2013].

[21] To determine how the short-term water vapor variability examined here relates to longer-term changes, we compare the vertical structure of specific humidity

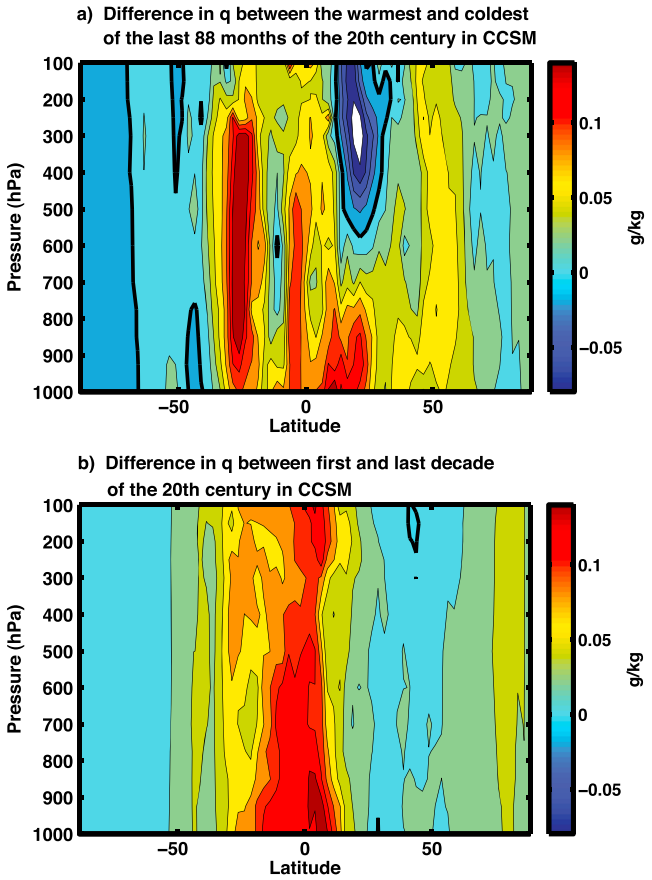

Figure 4. Zonally averaged vertical distribution in moisture anomaly for the Community Climate System Model (CCSM) (a) between the warmest and coldest decile of months in the last 88 months of the twentieth century integration of the CCSM, and (b) between the first and last decade of the twentieth century integration.

change between the first and last decades of a twentieth century simulation of the National Center for Atmospheric Research (NCAR) Community Climate System Model (CCSM) to the change between the coldest and warmest decile among the last 88 deseasonalized months of the same simulation, representing the time spanned by AIRS observations (Figure 4). We find that water vapor changes due to interannual variability exhibit regions of both moistening and drying (Figure 4a). In contrast, long-term transient warming results in a vertically uniform moistening of the tropical atmosphere (Figure 4b). This implies that the nature of the moisture perturbation forced by interannual variability is not the same as that resulting from a long-term forced change. The negative moisture anomaly is most pronounced in the upper troposphere near 25°N, a region with a large TOA effect (Figure 3), suggesting that our observational estimate of the water vapor feedback may be an underestimate of the longer-term feedback. This could be a source of systematic error in our analysis.

[22] There is also uncertainty associated with our choice of OLS regression. *Gregory et al.* [2004] demonstrate that OLS could be used to calculate the climate sensitivity of climate models. However, OLS does not account for uncertainty in our predictor variable, in this case, temperature. In reality, there is error associated with both temperature and water vapor measurements. Using total least squares regression, which assumes errors in both variables and minimizes the orthogonal distance to the regression line, leads to a much higher value for the water vapor feedback of 2.60 ± 0.21 $Wm^{-2}K^{-1}$. However, the radiative feedback framework we use assumes that water vapor is responding to the temperature change, plus some noise due to internal variability, so we are interested in the variability in atmospheric water vapor that is brought about by changes in surface temperature, and OLS regression is the most appropriate choice [see also *Gregory and Forster*, 2008]. As mentioned before, we have repeated our analysis with other surface temperature data sets, with similar results. This suggests that errors in global mean surface temperature may be less important than errors in water vapor retrievals.

5. CMIP3 Model Results

[23] In addition to using surface temperature data and satellite observations of moisture, we also employ twentieth century simulations from 14 atmosphere-ocean global climate models (AOGCMs) from the World Climate Research Programme's (WCRP) Coupled Model Intercomparison Project phase 3 (CMIP3) multimodel data set [*Meehl et al.*, 2007] in our analysis. Descriptions of the models used can be obtained from the CMIP3 archive (http://www-pcmdi.llnl.gov/ipcc/about_ipcc.php). The models chosen are the 14 models used in SH06. We use model-derived monthly averaged fields of water vapor for the entire twentieth century to derive dN_q from the radiation code, just as was done for AIRS. dN_q is then regressed against dT_s from the models. Values for Y_q for the 14 models, as well as the multimodel mean, are given in Table 1, where we include feedback values calculated by SH06 for comparison. The values obtained here by regression of twentieth century TOA flux anomalies generated using the ES radiation code are about 10% larger than those calculated by SH06, who carried out their calculations of water vapor feedback for the 21st century under increasing CO_2 emissions using the kernel technique. This difference is likely the result of a combination of differences in methodology and climate simulations used here and in SH06. At 10%, it is small enough that we can conclude that to first order, our results are in agreement with those of SH06.

Table 1. Water Vapor Feedback Estimates Derived Using Regression and Radiative Kernels[a]

Model Acronym	21st Century Kernel (SH06)	20th Century Regression	RMSE
CNRM	1.83	2.05	0.40
GFDL CM2_0	1.87	1.91	0.49
GFDL CM2_1	1.97	2.03	0.34
GISS AOM	2.14	2.31	1.55
GISS EH	1.99	1.88	0.80
GISS ER	1.86	1.79	1.22
INMCM3	1.56	1.98	0.24
IPSL	1.83	2.48	0.21
MIROC MEDRES	1.64	2.00	0.26
MRI	1.85	2.16	0.28
MPI ECHAM5	1.90	1.96	0.15
NCAR CCSM3	1.60	2.02	0.57
NCAR PCM1	1.48	2.02	0.33
UKMO HADCM3	1.67	1.80	0.27
Multi-model average	1.80	2.03	0.48
Range	1.48–2.14	1.79–2.49	
Standard error	0.08	0.05	

[a]Water vapor feedback from SH06 using the radiative kernel technique for a simulation of the 21st Century under increasing greenhouse gases (21st Century A1B Scenario with GFDL Kernel—first column), and the calculation of water vapor feedback for climate models using the twentieth century simulation and linear regression (Twentieth Century Regression—second column). The last column is the root-mean-square error in the regression-based calculation of feedback for an 88 month period relative to the entire twentieth century. The values in all columns have units of $W\ m^{-2}\ K^{-1}$. The mean, range, and standard error are included at the bottom of each column.

[24] Additionally, we use output from the 14 CMIP3 models to understand the dependence of the water vapor feedback magnitude on the length of time analyzed. The long global climate model time series allows us to examine the uncertainty in the calculation of the feedback parameter for the relatively short AIRS time series, assuming the relationships between feedback on different timescales in the model hold in reality. For each of the 100 year model simulations, we take 13 distinct 88 month time slices (corresponding to the length of the AIRS record) and calculate the feedback parameter for this subset. We estimate the error associated with the calculation of the short-term feedback parameter (Y_{short}) from our relatively short time series, as compared to the feedback parameter from the entire simulation (Y_{long}), by calculating the root-mean-square error ($\text{RMSE}_{\text{short}}$)

$$\text{RMSE}_{\text{short}} = \sqrt{\overline{(Y_{\text{short}} - Y_{\text{long}})^2}} \tag{4}$$

where the overbar represents an average over 13 different 88 month subsets of the total time series. The last column of Table 1 shows $\text{RMSE}_{\text{short}}$ in Y_q associated with taking the shorter time series for each of the models. We use the multimodel average of the $\text{RMSE}_{\text{short}}$, 0.48 $Wm^{-2}K^{-1}$, as an estimate for the error in our AIRS water-vapor feedback estimate associated with the short time record.

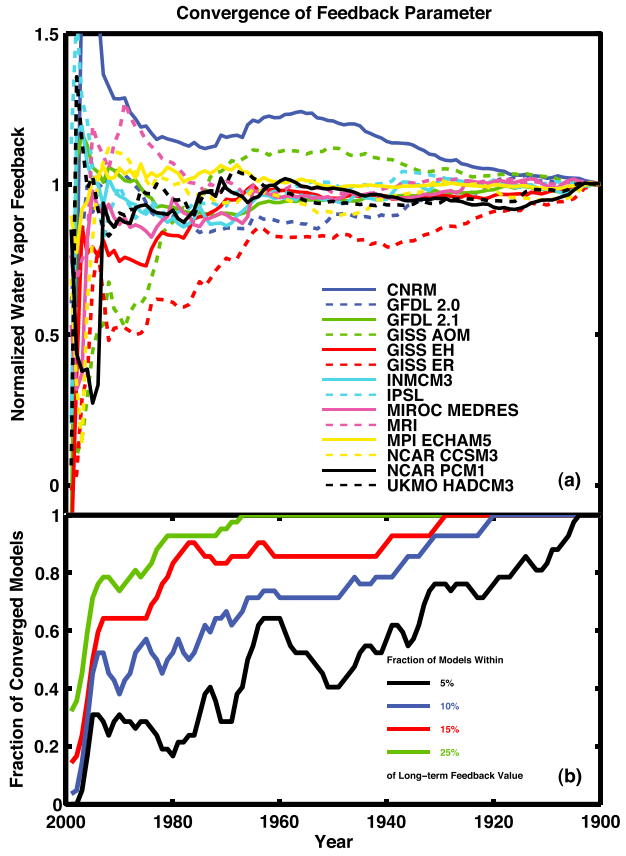

Figure 5. (a) Normalized water vapor feedback values for the 14 AOGCMs calculated using different record lengths, starting from the end of the record in year 2000 and proceeding back in time. Each value is normalized by the corresponding water vapor feedback for the entire twentieth century. (b) Fraction of models that attain a short-term feedback value within 5% (black), 10% (blue), 15% (red), and 25% (green) of the long-term value for each model. A 3 year box smoothing is applied to make the figure more readable.

[25] Figure 5a shows the value of the water vapor feedback derived from regression depending on the length of the time record used, starting from the end of the Twentieth Century in the year 2000. To estimate the length of record required for the short-term feedback calculation to yield results similar to those using the full time record, we calculate the fraction of models whose short-term water vapor feedback comes within a specified error range of the long-term feedback value (Figure 5b). For example, it takes 32 years before all models produce a short-term feedback that is within 25% of their long-term feedback value (green line in Figure 5b), while most (> 80%) models are within 15% of their final value after about 25 years (red line). Among the models, there is significant difference in the timescale over which the feedback value stabilizes, which could be due to many factors, including the differing internal variability characteristics of the models and differences in forcing used to drive the historical simulations. In addition, Figure 5a shows that some models from the same modeling centers behave differently, suggesting that changes in the model between versions can significantly impact their representations of processes associated with the water vapor feedback. This as well as the question whether newer model version from CMIP5 would have similar timescale dependence are interesting subjects to explore in future research.

[26] Figure 6 shows the feedback calculation for the entire twentieth century (Y_{long}), compared to the feedback calculated for 13 different 88 month subsets of the entire record (Y_{short}), for each of the 14 models (see legend). The value of Y_q from the AIRS observations, with the 95% confidence interval associated with the linear regression error, is represented by the yellow line and yellow shaded region (2.2 ± 0.4 $Wm^{-2}K^{-1}$). The blue line represents an OLS regression of Y_{short} versus Y_{long} for all models, and the blue shaded region bounds the 95% confidence for the slope and intercept of the regression line. The slope and intercept of this relationship are 1.92 ± 0.11 and -2.24 ± 0.23, respectively. There is typically a positive relationship between a model's long-term feedback and the feedback calculated using a shorter time series, but Y_{short} tends to underestimate Y_{long} for most realizations, in agreement with the 20 year

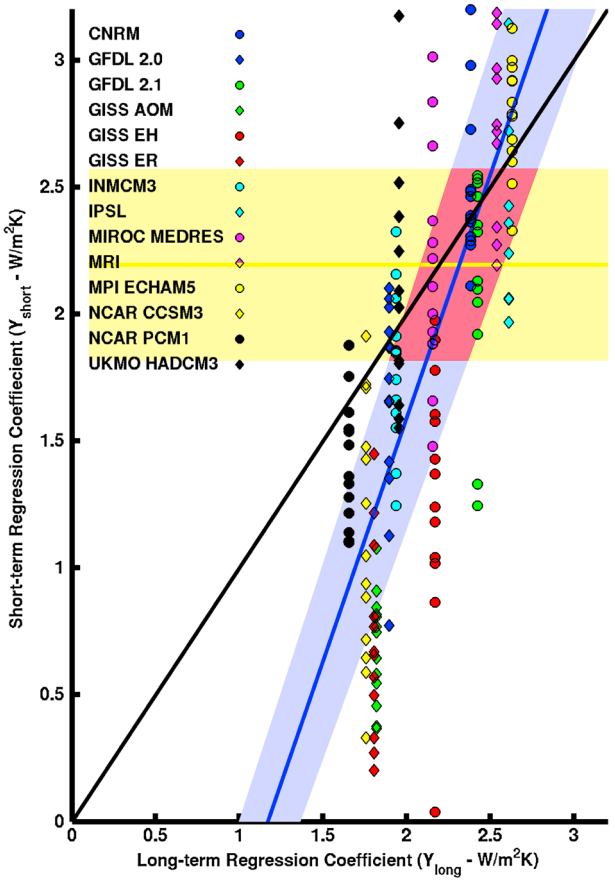

Figure 6. Comparison between the calculations of short-term water vapor feedback (Y_{short}) for distinct 88-month periods with the long-term water vapor feedback (Y_{long}) for 14 different AOGCMs. The blue line represents an ordinary least squares fit for all models, with the blue shaded region representing the 95% confidence interval for this regression. The solid black line is a one-to-one line for reference. The yellow shaded region represents the estimate in Y_q from the AIRS observations, with 95% confidence intervals. The red region represents an estimate of the range of possible values for the long-term water vapor feedback.

versus 100 year feedback comparison of *Dalton and Shell* [2013]. Averaged across all models used in this study, Y_{short} is about 75% of the value of Y_{long}. Since Y_{short} is dominated by internal variability, while Y_{long} includes a combination of internal variability and long-term forced climate change, this difference suggests that feedback behavior is not constant for all temporal scales and forcings. The red shaded region in Figure 6 shows our estimate of the long-term water vapor feedback constrained by observations, taking into account the error derived from the linear regression, the regression slope between the short-term and long-term feedback, and the error associated with this regression. The error analysis weights all models equally and does not account for possible nonlinearities that may result from differences in the responses of the present and possible future climates. This gives us a range of values for the observed long-term water vapor feedback of 1.9 to 2.8 $Wm^{-2}K^{-1}$.

6. Conclusions

[27] This work builds on previous attempts to constrain the water vapor feedback through observations [*Forster and Collins*, 2004; D08]. We have used the technique of linear feedback analysis, which has been shown to be effective in diagnosing climate feedback [*Forster and Gregory*, 2006; *Gregory and Forster*, 2008]. By forcing a radiative transfer model with the observed distribution of water vapor, we can understand the effect that the water vapor has on the TOA irradiance. Combining information on how global mean surface temperature affects the total atmospheric moisture content, we provide an estimate of the feedback that water vapor exerts in our climate system. Using our technique, we calculate a short-term water vapor feedback of 2.2 $Wm^{-2}K^{-1}$. The errors associated with this calculation, associated primarily with the shortness of our observational time series, suggest that the long-term water vapor feedback lies between 1.9 and 2.8 $Wm^{-2}K^{-1}$. The source of error from the relatively short time period is about three times as large as other error sources.

[28] The water vapor feedback derived in this work should be viewed cautiously as it is based on one 7 year realization of the climate system that could be anomalous and is likely dominated by short-term variability rather than long-term greenhouse gas induced warming. However, both the dry bias of the AIRS data used in this analysis and the heterogeneity of the interannual moisture perturbation in the short-term record suggest that our calculations provide an underestimate of the long-term water vapor feedback in response to transient warming. Thus, our results strengthen the case for a significantly positive feedback from water vapor changes in the climate system, which, acting alone, would double the magnitude of any warming forced by increasing greenhouse gas concentrations.

[29] **Acknowledgments.** We acknowledge the modeling groups, the Program for Climate Model Diagnosis and Intercomparison (PCMDI), and the WCRP's Working Group on Coupled Modelling (WGCM) for their roles in making available the WCRP CMIP3 multimodel data set. Support of this data set is provided by the Office of Science, U.S. Department of Energy. PF and NG were supported by NERC grant NE/E016189/1. NG was funded, in part, by the LLNL Institutional Postdoc Program. AJ was supported by NASA Grant NNX09AN92H and by the Office of Science (BER), U.S. Department of Energy, and KS by the National Science Foundation under Grant ATM 0904092, by NASA Grant NNH08CC72C, and by NorthWest Research Associates Inc.

References

Brohan, P., J. J. Kennedy, I. Harris, S. F. B. Tett, and P. D. Jones (2005), Uncertainty estimates in regional and global observed temperature changes: A new dataset from 1850, *J. Geophys. Res.*, *111*, D12106, doi:10.1029/2005JD006548.

Colman, R. (2003), A comparison of climate feedbacks in general circulation models, *Clim. Dyn.*, *20*, 865–873.

Colman, R. A., and L. I. Hanson (2013), On atmospheric radiative feedbacks associated with climate variability and change, *Clim. Dyn.*, *40*(1-2), 475–492, doi:10.1007/s00382-012-1391-3.

Colman, R. A., and B. McAvaney (2009), Climate feedbacks under a very broad range of forcing, *Geophys. Res. Lett.*, *36*, L01702, doi:10.1029/2008GL036268.

Colman, R. A., and S. B. Power (2009), Atmospheric radiative feedbacks associated with transient climate change and climate variability, *Clim. Dyn.*, *34*(7-8), 919–933, doi:10.1007/s00382-009-0541-8.

Dalton, M. M., and K. M. Shell (2013), Comparison of short-term and long-term radiative feedbacks and variability in 20th century global climate model simulations, *J. Clim.*, doi:10.1175/JCLI-D-12-00564.1, in press.

Dessler, A. E., Z. Zhang, and P. Yang (2008), Water-vapor climate feedback inferred from climate fluctuations, 2003–2008, *Geophys. Res. Lett.*, *35*, L20704, doi:10.1029/2008GL035333.

Edwards, J. M., and A. Slingo (1996), Studies with a flexible radiation code. I: Choosing a configuration for a large-scale model, *Q. J. R. Meteorol. Soc.*, *122*, 689–719.

Feigelson, E. D., and G. J. Babu (1992), Linear-regression in astronomy - II, *Astrophys. J.*, *397*, 55–67.

Fetzer, E. J., A. Eldering, E. F. Fishbein, T. Hearty, W. F. Irion, and B. Kahn (2005), Validation of AIRS/AMSU/HSB core products for data release version 4.0, *JPL D-31448*, 60 pp., Jet Propul. Lab., Pasadena, Calif.

Forster, P. M. D., and M. Collins (2004), Quantifying the water vapour feedback associated with post-Pinatubo global cooling, *Clim. Dyn.*, *23*, 207–214.

Forster, P. M. D., and J. M. Gregory (2006), The climate sensitivity and its components diagnosed from Earth radiation budget data, *J. Clim.*, *19*, 39–52.

Forster, P. M. D., and K. E. Taylor (2006), Climate forcings and climate sensitivities diagnosed from coupled climate model integrations, *J. Clim.*, *19*, 6181–6194.

Gettelman, A., and Q. Fu (2008), Observed and simulated upper-tropospheric water vapor feedback, *J. Clim.*, *21*, 3282–3289.

Gregory, J. M., W. J. Ingram, M. A. Palmer, G. S. Jones, P. A. Stott, R. B. Thorpe, J. A. Lowe, T. C. Johns, and K. D. Williams (2004), A new method for diagnosing radiative forcing and climate sensitivity, *Geophys. Res. Lett.*, *31*, L03205, doi:10.1029/2003GL018747.

Gregory, J. M., and P. M. Forster (2008), Transient climate response estimated from radiative forcing and observed temperature change, *J. Geophys. Res.*, *113*, D23105, doi:10.1029/2008JD010405.

Hall, A., and S. Manabe (1999), The role of water vapor feedback in unperturbed climate variability and global warming, *J. Clim.*, *12*, 2327–2346.

Held, I. M., and B. J. Soden (2000), Water vapor feedback and global warming, *Annu. Rev. Energy Environ.*, *25*, 441–475.

Jonko, A. K., K. M. Shell, B. M. Sanderson, and G. Danabasoglu (2013), Climate feedbacks in CCSM3 under changing CO_2 forcing. Part II: Variation of climate feedbacks and sensitivity with forcing, *J. Clim.*, *26*, 2784–2795.

Meehl, G. A., C. Covey, T. Delworth, M. Latif, B. McAvaney, J. F. B. Mitchell, R. J. Stouffer, and K. E. Taylor (2007), THE WCRP CMIP3 multi-model dataset: A new era in climate change research, *Bull. Am. Meteorol. Soc.*, *88*, 1383–1394, doi:10.1175/BAMS-88-9-1383.

Murphy, D. M., and P. M. Forster (2010), On the accuracy of deriving climate feedback parameters from correlations between surface temperature and outgoing radiation, *J. Clim.*, *23*, 4983–4988, doi:10.1175/2010JCLI3657.1.

Rap, A., P. M. Forster, A. Jones, O. Boucher, J. M. Haywood, N. Bellouin, and R. R. De Leon (2010), Parameterization of contrails in the UK Met Office Climate Model, *J. Geophys. Res.*, *115*, D10205, doi:10.1029/2009JD012443.

Rossow, W. B., and R. A. Schiffer (1999), Advances in understanding ISCCP, *Bull. Am. Meteorol. Soc.*, *80*, 2261–2287.

Shell, K. M., J. T. Kiehl, and C. A. Shields (2008), Using the radiative kernel technique to calculate climate feedbacks in NCAR's Community Atmospheric Model, *J. Clim.*, *21*, 2269–2282.

Soden, B. J. (1997), Variations in the tropical greenhouse effect during El Niño, *J. Clim.*, *10*, 1050–1055.

Soden, B. J., R. T. Wetherald, G. L. Stechikov, and A. Robock (2002), Global cooling after the eruption of Mount Pinatubo: A test of climate feedback by water vapor, *Science*, *297*, 727–730.

Soden, B. J., and I. M. Held (2006), An assessment of climate feedbacks in coupled ocean-atmosphere models, *J. Clim.*, *19*, 3354–3360.

Soden, B. J., I. M. Held, R. Colman, K. M. Shell, J. T. Kiehl, and C. A. Shields (2008), Quantifying climate feedbacks using radiative kernels, *J. Clim.*, *21*, 3504–3520.

Spencer, R. W., and W. D. Braswell (2008), Potential biases in feedback diagnosis from observational data: A simple model demonstration, *J. Clim.*, *21*, 5624–5628.

Susskind, J., C. D. Barnet, and J. M. Blaisdell (2003), Retrieval of atmospheric and surface parameters from AIRS/AMSU/HSB data in the presence of clouds, *IEEE Trans. Geosci. Remote Sens.*, *41*, 390–409.

Wetherald, R. T., and S. Manabe (1988), Cloud feedback processes in a general circulation model, *J. Atmos. Sci.*, *45*, 1397–1415.

Uppala, S. M., et al. (2005), The ERA-40 reanalysis, *Q. J. R. Meteorol. Soc.*, *131*, 2961–3012.